

Article

Co-Estimation of State-of-Charge and State-of-Health for High-Capacity Lithium-Ion Batteries

Ran Xiong ¹, Shunli Wang ^{1,*} , Fei Feng ^{2,*}, Chunmei Yu ¹, Yongcun Fan ¹, Wen Cao ¹ and Carlos Fernandez ³ 

¹ School of Information Engineering, Southwest University of Science and Technology, Mianyang 621010, China; xiongran@mails.swust.edu.cn (R.X.); yuchunmei@swust.edu.cn (C.Y.); ycfan@swust.edu.cn (Y.F.); caowen@swust.edu.cn (W.C.)

² School of Automation, Chongqing University, Chongqing 400044, China

³ School of Pharmacy and Life Sciences, Robert Gordon University, Aberdeen AB10-7GJ, UK; c.fernandez@rgu.ac.uk

* Correspondence: wangshunli@swust.edu.cn (S.W.); feifeng@cqu.edu.cn (F.F.)

Abstract: To address the challenges of efficient state monitoring of lithium-ion batteries in electric vehicles, a co-estimation algorithm of state-of-charge (SOC) and state-of-health (SOH) is developed. The algorithm integrates techniques of adaptive recursive least squares and dual adaptive extended Kalman filtering to enhance robustness, mitigate data saturation, and reduce the impact of colored noise. At 25 °C, the algorithm is tested and verified under dynamic stress test (DST) and Beijing bus DST conditions. Under the Beijing bus DST condition, the algorithm achieves a mean absolute error (MAE) of 0.17% and a root mean square error (RMSE) of 0.19% for SOC estimation, with a convergence time of 4 s. Under the DST condition, the corresponding values are 0.05% for MAE, 0.07% for RMSE, and 5 s for convergence time. Moreover, in this research, the SOH is described as having internal resistance. Under the Beijing bus DST condition, the MAE and the RMSE of the estimated internal resistance of the proposed approach are 0.018% and 0.075%, with the corresponding values of 0.014% and 0.043% under the DST condition. The results of the experiments provide empirical evidence for the challenges associated with the efficacious estimation of SOC and SOH.



Citation: Xiong, R.; Wang, S.; Feng, F.; Yu, C.; Fan, Y.; Cao, W.; Fernandez, C. Co-Estimation of State-of-Charge and State-of-Health for High-Capacity Lithium-Ion Batteries. *Batteries* **2023**, *9*, 509. <https://doi.org/10.3390/batteries9100509>

Academic Editor: Catia Arbizzani

Received: 11 August 2023

Revised: 6 October 2023

Accepted: 10 October 2023

Published: 12 October 2023



Copyright: © 2023 by the authors. Licensee MDPI, Basel, Switzerland. This article is an open access article distributed under the terms and conditions of the Creative Commons Attribution (CC BY) license (<https://creativecommons.org/licenses/by/4.0/>).

Keywords: state-of-charge; state-of-health; adaptive recursive least squares; dual adaptive extended Kalman filtering

1. Introduction

In response to energy depletion and environmental protection issues, electric vehicles (EVs) are considered popular alternatives to traditional fossil fuel vehicles [1,2]. Compared with gasoline vehicles, EVs have many advantages, including low noise emissions, low pollution, and high power efficiency [3]. EVs are the key technology used to solve the problem of carbon dioxide emissions, and the core component that EVs rely on is the battery [4–6]. Among them, lithium-ion (Li-ion) batteries are widely employed on account of their electrochemical energy storage properties [7,8]. Li-ion batteries offer several advantages, including high portability, high performance after hundreds or thousands of at least partial cycles, and high power density [9,10]. The security and effective management of Li-ion batteries are closely related to their available maximum capacity and cycle life [11]. According to the current technological situation, the technologies applied in Li-ion batteries are not enough, and there are still many problems that wait to be solved. Unsafe accidents such as battery leakage, battery explosion, battery fire, etc. occur from time to time. Therefore, the high-efficiency application and maintenance technology of Li-ion batteries has become a research hotspot. Enhancing the reliability, safety, and longevity of Li-ion batteries has emerged as a pressing concern, necessitating immediate attention. To ensure the security, efficiency, and normal operation of Li-ion batteries, the implementation of effective battery management becomes paramount [12–15]. In practical applications, cells

are commonly interconnected in series and parallel configurations to create systems [16]. This arrangement allows for the desired voltage and current requirements to be achieved while accommodating the specific needs of the application. With series-connected structure, the pack voltage can be increased, while connecting cells in parallel enables the total capacity to be augmented. This series-parallel connection scheme offers flexibility and customization in designing battery systems that meet the power and energy demands of various applications. Consequently, the establishment of a battery management system (BMS) becomes crucial to supervise and control the conditions of each individual cell, ensuring the optimal performance of the running system [17–20]. The SOC and SOH are the two primary battery states that have significant implications for the safety of the BMS and the operational state of EVs [21,22]. The general models used for the determination of micro-health parameters include the pseudo-two-dimensional (P2D) model and its simplification models. A representative simplified model is based on the Padé approximation [23]. In addition, other simplification models, such as the single-particle model and the extended single-particle model, are common and widely adopted. Precise estimation and prediction of the SOC and SOH are instrumental in optimizing the BMS to extend cycle life and reduce battery replacement costs [24–26].

Indeed, directly measuring the SOC and SOH of a battery using a simple instrument can be challenging. Therefore, it is a more reasonable way to estimate these two states through related parameters [27]. At present, there are many algorithms for estimating SOC and SOH, which usually incorporate direct methods, data-driven methods, physical model-based methods, and hybrid model-based methods. Direct methods contain ampere-hour integration, open circuit voltage (OCV), and electrochemical impedance spectroscopy (EIS). Among the methods used for SOC estimation, the ampere-hour integration method can be very sensitive to the initial SOC, the OCV method requires the battery to be at rest for a significant time to stabilize and for the OCV-SOC relationship to be established, and the EIS method requires a very complicated electrochemical theory to perform state estimation [28–34]. The strength of the data-driven methods is that there is no requirement for an accurate model, and the disadvantage is that the amount of the experimental data is huge and the training process is complicated and cumbersome. In recent years, common data-driven methods in the literature include fuzzy control [35], relevance vector machines [36], support vector machines [37–39], Gaussian process regression [40], neural networks [41–45], and other deep learning methods [46–48]. Houde Dai et al. introduced a new estimation approach for the SOC and SOH by leveraging neural networks with prior information and Markov chain analysis [49]. Runnan Zhang et al. employed a co-estimation approach of the SOC and the temperature for a lithium iron phosphate battery based on ultrasonic reflection waves. In this method, the ultrasonic technique and the backpropagation network were used [50]. Data-driven methods for the SOC and SOH estimation are making continuous progress; they do not rely on physical models, and the estimation results may have large deviations. On the other side, the equivalent circuit model (ECM) is the most common physical model, and it can indeed be utilized for the estimation of SOC and SOH by combining with some filtering methods and identification methods. Among the filtering methods, Kalman filtering and particle filtering are the most commonly used. However, the time consumed by the particle filtering calculation is much greater than the time consumed by the extended Kalman filtering (EKF), and the calculation time of the particle filtering increases approximately in series with the increase in the number of particles. Therefore, the estimation methods based on the Kalman algorithm are the most suitable for experimental research. Certainly, based on EKF, various research studies have explored different algorithms and methods for jointly estimating the SOC and SOH of batteries. For instance, Jiabo Li et al. investigated a dual extended Kalman filtering (DEKF) algorithm for the joint estimation of SOC and SOH [51]. In reference document [26], a co-estimation method of SOC and SOH was analyzed based on the DEKF and a multivariate autoregressive model. Qiao Zhu et al. employed a fractional-order adaptive extended Kalman filtering (AEKF) approach for estimating SOC [52]. It leverages fractional order modeling and adaptive

filtering techniques to estimate SOC more effectively. In [53], Yigang Li et al. drew upon a SOC estimation method based on bias compensation recursive least squares. The reference document [54] found a forgetting factor recursive least squares method to estimate battery SOC. This method incorporates a forgetting factor in the recursive least squares algorithm to adaptively update the SOC estimation and improve its accuracy over time. To estimate the state with unknown model parameters, Qizhe Lin et al. combined the second-order RC ECM and the eXogenous Kalman filter [55]. Moreover, a robust state-space filter that has a Kalman-like structure can also be used here [56]. To simultaneously estimate state trajectories and model parameters, Reference document [57] and Reference document [58] made some contributions. Specifically, reference document [58] proposed a robust fixed-lag smoothing method under model perturbations, and Reference document [57] developed a new adaptive algorithm based on combined direct reactive power control and fuzzy logic control techniques. However, the above methods do not take into account the effects of colored noise and data saturation on the estimation results, which greatly affects the estimation performance. White noise is often used for calculations in previous research, but ideal white noise is difficult to achieve physically, and the noise contained in measured data in engineering practice is colored noise. That is to say, noise in the real world belongs to colored noise. In practical applications, the recursive least squares (RLS) method may experience data saturation, which mainly refers to the accumulation of old data as the number of iterations increases, resulting in the flooding of new data information. This ultimately leads to parameter estimation being impossible and algorithm failure. Building upon the improvement of the Kalman filtering algorithm, by combining some strong points of reference documents [51–56], an adaptive co-estimation algorithm is proposed, which is named the forgetting factor bias compensation recursive least squares-dual adaptive extended Kalman filtering (FBC-DAEKF) algorithm.

The main motivation to encourage this research is the current demand for more effective state estimation in Li-ion batteries under operation. This motivation can also reflect the impact of the work on the related research field. In this research, a fresh co-estimation algorithm for the SOC and SOH of batteries is developed under full consideration of the source of errors. The algorithm utilizes the FBC method to identify unknown parameters in the Thevenin ECM online, and the internal resistance is employed to describe the battery SOH. The proposed algorithm addresses several challenges commonly encountered in SOC and SOH estimation. It incorporates two adaptive extended Kalman filters to estimate SOC and internal resistance. The algorithm takes into account issues such as data saturation, interference from system-colored noise, and changes in observation noise. To mitigate data saturation and interference from system-colored noise, the algorithm introduces a forgetting factor and bias compensation based on the recursive least squares method. These techniques help to adjust system noise parameters and compensate for biases, improving estimation accuracy. Additionally, adaptive filters are employed to account for changes in observation noise characteristics. These filters enable the algorithm to adjust the noise parameters based on a statistical analysis of time-varying noise characteristics. Test results demonstrate that the developed co-estimation algorithm is not dependent on the initial values of SOC and SOH. Even when the initial values are given incorrectly, the algorithm exhibits rapid convergence to the reference values with higher estimation accuracy compared to traditional algorithms. Overall, the research presents a comprehensive co-estimation method for SOC and SOH, addressing key challenges and demonstrating improved estimation accuracy. The proposed algorithm offers potential advancements in BMSs and contributes to the reliable and efficient operation of batteries.

The subsequent sections are structured as follows: Section 2 provides a comprehensive mathematical analysis, covering equivalent modeling, the formula derivation for the parameter identification method, and the iterative calculation process for SOC and internal resistance. The details of relevant experimental results are described in Section 3. Lastly, in Section 4, the main conclusions drawn from the entire paper are summarized.

2. Materials and Methods

2.1. Modeling of Battery Equivalent Circuit

Before estimating the battery state, it is crucial to develop an appropriate battery model. Battery models can generally be classified into three types, covering electrochemical models (EMs), neural network (NN) models, and ECMs [59–61]. Among them, the modeling and computation of EMs pose significant challenges and may not be readily applicable to a wide range of engineering applications. The development of NN models necessitates extensive experimental data to ensure reliability, but it is susceptible to large errors. The ECMs simulate the battery voltage characteristics based on circuit elements such as power supply, inductance, capacitance, and resistance without considering the chemical composition and corresponding reactions inside the batteries. While a simplistic model offers ease of computation, it falls short of accurately depicting the intricate operational traits of the battery. Conversely, a more intricate model enables a more precise characterization of the battery's charging and discharging behavior, albeit at the expense of significantly heightened computational requirements. The Thevenin model considers the two nonlinear parameters of plate equivalent capacitance and electrolyte and nonlinear contact resistance on the basis of an ideal ECM [15]. The Thevenin model exhibits remarkable efficacy in capturing both the dynamic and static attributes of lithium batteries. Its widespread utilization in estimating the SOC and SOH stems from its advantageous combination of low computational complexity and high accuracy. As a result, the present study adopts the Thevenin model, which is depicted in Figure 1.

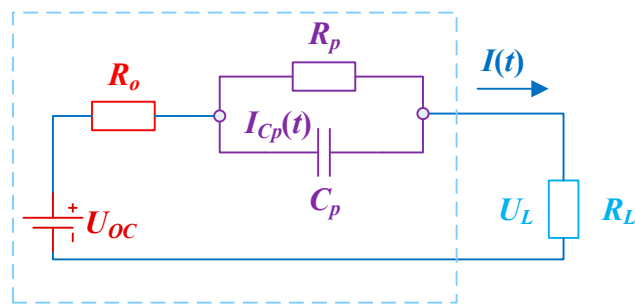


Figure 1. Thevenin ECM.

Within the model, two crucial parameters are employed: R_o and R_p , denoting the internal resistance pertaining to ohmic and polarization effects, respectively. Additionally, C_p symbolizes the polarization capacitance, while U_L signifies the circuit's battery terminal voltage. In this circuit, R_o can be used to describe the instantaneous change of U_L . Furthermore, R_p and C_p serve as indicators of the polarization reaction within the battery. By adhering to the principles of the Thevenin model and Kirchhoff's law, the mathematical depictions of this circuit can be expressed as follows:

$$\begin{cases} U_{oc} = U_L + U_p + U_o \\ I = \frac{U_p}{R_p} + \frac{C_p dU_p}{dt} \end{cases} \quad (1)$$

Wherein U_p denotes the voltage of R_p and C_p , U_{oc} signifies the OCV, U_o denotes the voltage of R_o , and I denotes the current passing through the entire Thevenin circuit. The generally accepted definition of SOC is shown below.

$$\begin{cases} SOC_t = SOC_{t_0} - \frac{\int_{t_0}^t \eta I(t) dt}{Q_0} \\ OCV = f(SOC) \end{cases} \quad (2)$$

Among them, Q_0 describes the rated capacity, while η denotes the Coulomb efficiency coefficient. The value of internal resistance is adopted to describe the SOH. In addition,

the battery OCV can be fitted by SOC to correct the model and algorithms. Combining Equation (2) and the theory of control equations, the state space and observation equations for Li-ion battery cells can be derived, yielding the following expressions [15].

$$\begin{cases} \begin{bmatrix} SOC_{k+1} \\ U_{p,k+1} \end{bmatrix} = \begin{bmatrix} 1 & 0 \\ 0 & e^{-\frac{T}{R_p}} \end{bmatrix} \begin{bmatrix} SOC_k \\ U_{p,k} \end{bmatrix} + \begin{bmatrix} -\frac{T}{Q_N} \\ R_p(1 - e^{-\frac{T}{R_p}}) \end{bmatrix} I_k + \begin{bmatrix} w_{1,k} \\ w_{2,k} \end{bmatrix} \\ U_{L,k} = U_{oc,k} - R_o I_k + [0 - 1] \begin{bmatrix} SOC_k \\ U_{p,k} \end{bmatrix} + v_k \end{cases} \quad (3)$$

Among them, T represents the sampling interval of the experimental instrument, w_1 and w_2 are the state errors of SOC and U_p , and v describes the measurement error of U_L .

2.2. FFBCRLS Parameter Identification

Parameter identification is a vital procedure conducted after the conclusion of an experimental study. The outcome of parameter identification holds significant importance in establishing an accurate battery model. Identification methods basically include off-line algorithms and online algorithms. On the one hand, the offline algorithms calculate model parameters through formulas, and this method is only applicable to specific models. On the other hand, the online identification algorithms obtain model parameters in real time through data fitting. This method is suitable for most battery models and has high accuracy and strong versatility. Therefore, the identification method used in this paper is an online algorithm named the forgetting factor bias compensation recursive least squares (FBC) method. It not only minimizes the error associated with the discharge rate change in identification but also effectively reduces the identification error caused by the colored noise of the system and strengthens the impact of new data, which is the ability that the recursive least squares (RLS) method does not have. Based on the Thevenin ECM, the formula for the battery terminal voltage and its Laplace transformation equation are described as follows:

$$\begin{cases} U_{oc} = U_L + U_p + U_o \\ U_{oc}(s) = U_L(s) - I(s) \left(\frac{R_p}{1 + R_p C_p s} + R_o \right) \end{cases} \quad (4)$$

By performing a z-transform on the Laplace transformation equation of Equation (4), after discretization, the transfer equation can be derived, as illustrated below:

$$\begin{cases} G(s) = \frac{\frac{R_o T + R_p T + 2R_p C_p R_o}{T + 2R_p C_p} + \frac{R_o T + R_p T - 2R_p C_p R_o}{T + 2R_p C_p} z^{-1}}{1 + \frac{T - 2R_p C_p}{T + 2R_p C_p} z^{-1}} \\ \frac{U_L(s) - U_{oc}(s)}{I(s)} = \frac{E(s)}{I(s)} = G(s), s = \frac{2(1 - z^{-1})}{T(1 + z^{-1})} \end{cases} \quad (5)$$

According to Equation (4), the simplified difference equation can be represented using a bilinear transformation, as demonstrated below:

$$y(k) = -ay(k-1) + bu(k) + cu(k-1) + v(k) \quad (6)$$

Among them, the values of the parameters included are unknown and required to be estimated. Furthermore, $v(k)$ represents the error of the vector equation. To facilitate calculations and adhere to the principles of RLS, the least squares form can be discretely expressed in vector mode on the basis of Equation (6), as shown below:

$$\begin{cases} y(k) = x(k)^T \theta(k) + v(k) \\ x(k) = [y(k-1) u(k) u(k-1)]^T \\ \theta_c(k) = [-a \ b \ c]^T \end{cases} \quad (7)$$

Drawing upon the principles of RLS and the Thevenin circuit, the values of a , b , and c in the above equations can be calculated, respectively, as shown below:

$$\begin{cases} a = \frac{T - 2\tau}{T + 2\tau} \\ b = \frac{R_o T + R_p T + 2\tau R_o}{T + 2\tau} \\ c = \frac{R_o T + R_p T - 2\tau R_o}{T + 2\tau} \end{cases} \quad (8)$$

Among them, τ represents the RC time constant, while T denotes the sampling interval. According to Equations (7) and (8), R_o , C_p , and R_p can be derived, which can be expressed as follows:

$$\begin{cases} R_o = \frac{b - c}{1 - a} \\ \tau = R_p C_p = \frac{1 - a}{2a + 2} \\ R_p = (1 + 2\tau)b - 2R_o\tau - R_o \\ C_p = \frac{\tau}{R_p} \end{cases} \quad (9)$$

The above-mentioned RLS method for real-time parameter identification can ensure the accuracy of results under stable working conditions and environments. Equation (7) is the expression of least squares. The forgetting factor recursive least squares (FFRLS) approach proves effective in mitigating data saturation. The formulas employed to calculate the parameters of the RC circuit through the FFRLS method are presented below:

$$\begin{cases} \theta(k) = \theta(k - 1) + KP(k - 1)x(k)[y(k) - x(k)^T\theta(k - 1)] \\ K = [x(k)^T P(k - 1)x(k) + \lambda]^{-1} \\ P(k) = \lambda^{-1}[I - KP(k - 1)x(k)x(k)^T]P(k - 1) \end{cases} \quad (10)$$

However, the FFRLS method cannot effectively overcome the interference of the system-colored noise because it is a biased estimation method in this situation. Hence, in this paper, the FBC method is introduced as an online parameter identification approach to address the aforementioned issues. When the system noise exhibits colored characteristics, the estimation obtained from the RLS method is prone to bias, so a bias compensation item should be added to the estimated equation to make the estimation result an unbiased estimation. Therefore, a least squares (LS) cost function is required to be constructed, as shown below:

$$\begin{cases} \zeta(k) = y(k) - x^T(k)\hat{\theta}(k - 1) \\ \varepsilon(k, i) = y(i) - x^T(i)\hat{\theta} \\ J(k) = \sum_{i=1}^k \lambda^{k-i} [\zeta(i) - x^T(i)\theta]^2 \end{cases} \quad (11)$$

Among them, ζ represents the innovation of the observations. ε represents the residuals of observations, and J is the LS cost function. In Equations (10) and (11), the following equations can be derived to prepare for deriving the recursive process of J . The specific equations are shown below:

$$\begin{cases} J(k) = \sum_{i=1}^k \lambda^{k-i} \varepsilon^2(k, i) = \sum_{i=1}^{k-1} \lambda^{k-i} \varepsilon^2(k, i) + \varepsilon^2(k, k) \\ = \sum_{i=1}^{k-1} \lambda^{k-i} \varepsilon^2(k - 1, i) + \sum_{i=1}^{k-1} \lambda^{k-i} [x^T(i)K(t)]^2 \zeta^2(t) \\ - 2 \sum_{i=1}^{k-1} \lambda^{k-i} \varepsilon^2(k - 1, i) x^T(i)K(t)\zeta(t) + \varepsilon^2(k, k) \\ \sum_{i=1}^{k-1} \varepsilon^2(k - 1, i) x^T(i) = 0 \\ K^T(k)P(k - 1)K(k) = \frac{x^T(k)P(k - 1)x(k)}{[\lambda + x^T(k)P(k - 1)x(k)]^2} \\ \varepsilon(k, k) = \frac{\zeta(k)}{\lambda + x^T(k)P(k - 1)x(k)} \end{cases} \quad (12)$$

Substituting the second equation in Equation (12) into the first equation, it can be seen that the third item on the right of the first formula equals zero, and then substituting the third and fourth equations in Equation (12) into the first equation, the recursive process of J can be obtained, as shown below:

$$J(k) = \lambda J(k-1) + \frac{[y(k) - x^T(k)\hat{\theta}(k-1)]^2}{\lambda + x^T(k)P(k-1)x(k)} \quad (13)$$

In order to estimate the variance of voltage noise, there should be an equation related to the LS cost function to derive the variance. Therefore, the relevant equation can be derived from the minimum value of J , which is demonstrated as follows:

$$\lim_{k \rightarrow \infty} \frac{1}{k} J(k) = \sigma^2 \left[1 + \left(\lim_{k \rightarrow \infty} \hat{\theta}(k) \right)^T \hat{\theta}_c \right] \quad (14)$$

Among them, σ^2 is the variance of voltage noise, and θ_c is the estimated result of the FBC method. θ_c adds a bias compensation term on the basis of the unbiased estimation result θ . By seeking the limit of Equation (14), an equation of variance with respect to the LS cost function can be obtained. Thus, the whole recursive process of the FBC method can be depicted as follows [62]:

$$\left\{ \begin{array}{l} \theta(k) = \theta(k-1) + KP(k-1)x(k)[y(k) - x^T(k)\theta(k-1)] \\ K = [x^T(k)P(k-1)x(k) + \lambda]^{-1} \\ P(k) = \lambda^{-1}[I - K \cdot P(k-1)x(k)x^T(k)]P(k-1) \\ J(k) = \lambda J(k-1) + \frac{[y(k) - x^T(k)\theta(k-1)]^2}{\lambda + x^T(k)P(k-1)x(k)} \\ \sigma^2(k) = \frac{J(k)}{k[1 + \theta_c(k-1)D\theta(k)]} \\ D = \begin{bmatrix} I_n & 0 \\ 0 & 0 \end{bmatrix} \\ \theta_c(k) = \theta(k) + k\sigma^2(k)P(k)D\theta_c(k-1) \end{array} \right. \quad (15)$$

Among them, the forgetting factor serves to diminish the impact of older data while reinforcing the feedback effect of newer data. Furthermore, the introduction of bias compensation can strengthen the method's suppression effect on the system-colored noise interference, thereby reducing the estimated errors caused by the biased estimation.

2.3. Principle of the DAEKF Approach

Currently, various approaches for estimating battery SOC and SOH can be found in the literature. These methods include the direct method, data-driven methods, the particle filtering method, the Kalman filtering method, and various enhanced techniques derived from them. However, because of the inherent nonlinearity of the battery system, SOC and SOH estimation are prone to noise interference.

In recent years, the estimation of battery states drawing upon data-driven methods has become a new trend, but the prerequisite for using such methods requires the accumulation of massive historical data. In experimental research, optimized approaches based on classical methods such as Kalman filtering and particle filtering are the commonly used algorithms for state estimation.

Among the aforementioned improved methods, the EKF algorithm linearizes the state equation, followed by the utilization of the Kalman filtering algorithm for computation. In this study, a novel approach is developed that integrates two extended Kalman filters, incorporating the concepts of forgetting factor and bias compensation, to estimate both the SOC and internal resistance. In addition, both of the extended Kalman filters are combined with an adaptive filter. Compared with the EKF algorithm, the proposed method has the following two advantages: Firstly, the introduction of a FBC method can overcome the

problems of data saturation and interference from system-colored noise. Secondly, adaptive filters are employed to predict and correct the real-time observation noise.

The Kalman filtering method recursively estimates the current state according to the input and output of the system by establishing linear state-space equations. It is worth noting that it is entirely based on time domain estimation. Consequently, it only entails relatively low computational requirements. This algorithm is a recursive and reliable autoregressive data processing technique, primarily suitable for linear systems. By employing linear discretization processing, the equations of state and observation can be expressed below:

$$\begin{cases} x_k = A_{k-1}x_{k-1} + B_{k-1}u_{k-1} + w_{k-1} \\ y_k = C_{k-1}x_k + D_ku_k + w_k \end{cases} \quad (16)$$

Among them, k represents the sample time, A denotes the transfer coefficient of x , B signifies the system control input coefficient, C symbolizes the system measurement coefficient, D stands for the feedforward coefficient, and u is described for the system input variable. Furthermore, x and y represent the state variable and the observed value of the system, respectively.

In the EKF method, the state matrix incorporates the SOC as one of its components. Building upon this, the current and the terminal voltage are employed as input and output. Within the state-space equations, the predicted state equation incorporates the definition of ampere-hour integration, and the observation equation reflects the simulated terminal voltage of the ECM. When using this algorithm to estimate SOC, the establishment of ECM leads to a substantial influence on the estimation results. The discrete equations of state and observation in the state-space representation are presented below:

$$\begin{cases} X_{k+1} = f(X_k, k) + w_k \\ Z_k = h(X_k, k) + v_k \end{cases} \quad (17)$$

Among them, k is the sampling time, X and Z are the state variable and observation value, and their corresponding errors are w and v , respectively. Both w and v are described in this study as independent Gaussian white noises. For addressing nonlinear issues, the first-order expansion can simplify the expression of Kalman filtering. The simplified expressions are shown below:

$$\begin{cases} f(X_k, k) \approx f(\hat{X}_k, k) + \frac{\partial f(X_k, k)}{\partial X_k} \Big|_{X_k=\hat{X}_k} (X_k - \hat{X}_k) \\ h(X_k, k) \approx h(\hat{X}_k, k) + \frac{\partial h(X_k, k)}{\partial X_k} \Big|_{X_k=\hat{X}_k} (X_k - \hat{X}_k) \end{cases} \quad (18)$$

Through a series of shift changes and assignment processing, the space expressions of the following four matrices can be obtained, which are shown below:

$$\begin{cases} A_k = \frac{\partial f(X_k, k)}{\partial X_k} \Big|_{X_k=\hat{X}_k}, B_k = f(\hat{X}_k, k) - A_k \hat{X}_k \\ C_k = \frac{\partial h(X_k, k)}{\partial X_k} \Big|_{X_k=\hat{X}_k}, D_k = h(\hat{X}_k, k) - C_k \hat{X}_k \end{cases} \quad (19)$$

Combining Equations (17) and (19), the nonlinear expression can be simplified to a linear expression, as shown below:

$$\begin{cases} X_{k+1} = A_k X_k + B_k + w_k \\ Z_k = C_k X_k + D_k + v_k \end{cases} \quad (20)$$

After obtaining the expression of the linear system, by initializing the state variables and their variances, the EKF algorithm can be applied to the discrete system for estimating state variables. Since SOC and SOH need to be estimated simultaneously, the DEKF approach is introduced. The first filter is utilized for the SOC estimation, while the second filter is employed for the ohmic internal resistance estimation. The two filters are coupled

to each other and affect each other. By estimating the value of the ohmic internal resistance, the corresponding SOH estimation results can be calculated through the internal resistance definition.

Since the EKF algorithm cannot make noise adaptive, this paper introduces two adaptive filters with the ability to count the characteristics of time-varying noise into DEKF. Each adaptive filter makes an unbiased estimation based on the statistically large posterior suboptimal of the measured value. The updated equations for process noise Q and observation noise R can be illustrated below:

$$\begin{cases} \hat{Q}_{k+1} = \frac{1}{k+1} G \sum_{i=0}^k \left(K_{k+1} \tilde{\gamma}_{k+1} \tilde{\gamma}_{k+1}^T K_{k+1}^T + P_{k+1} - AP_{k+1}A^T \right) G^T \\ G = (\Gamma^T \Gamma)^{-1} \\ \hat{R}_{k+1} = \frac{1}{k+1} \sum_{i=0}^k \left(\tilde{\gamma}_{k+1} \tilde{\gamma}_{k+1}^T - CP_{k+1}A^T C^T \right) \end{cases} \quad (21)$$

Through the incorporation of adaptive filters, the algorithm developed in this paper enables real-time updates of the noise parameters Q and R . This continuous revision of the joint estimation results facilitates the optimization of the estimation outcomes. By combining the DEKF algorithm with the adaptive filtering algorithm, the recursive calculation process of the DAEKF algorithm is represented as follows:

$$\begin{cases} \hat{X}_{k+1}^- = f(\hat{X}_k) \\ \hat{P}_{k+1}^- = A_k \hat{P}_k A_k^T + \Gamma Q_{k+1} \Gamma^T \\ K_{k+1} = \hat{P}_{k+1}^- C_{k+1}^T \left(C_{k+1} \hat{P}_{k+1}^- C_{k+1}^T + R_{k+1} \right)^{-1} \\ \hat{X}_{k+1} = X_{k+1}^- + K_{k+1} [Z_{k+1} - h(X_{k+1}^-)] \\ \hat{P}_{k+1} = [I - K_{k+1} C_{k+1}] P_{k+1}^- \end{cases} \quad (22)$$

Among them, Γ represents the noise-driven matrix, k signifies the sample time, \hat{X}^- and \hat{P}^- denote the prior state and covariance error, and K stands for the corresponding Kalman gain. In addition, \hat{X} and \hat{P} symbolizes the posterior state and covariance error. Q and R indicate the related matrices of w and v , while I represents a unit matrix.

2.4. Calculation Process of the DAEKF Approach

Based on the above analysis, it is evident that when employing the FBC-DAEKF algorithm for estimating SOC and ohmic internal resistance, the related equations of state and observation are expressed as follows:

$$\begin{cases} x(k|k-1) = A_{k-1}^x x(k-1) + B_{k-1}^x i_{k-1} + w_k \\ y_k = h(x_{k-1}, i_{k-1}) + v_k = U_{oc} - R_p i_k - u_k + v_k \end{cases} \quad (23)$$

Combining Equations (3) and (23), it can be known that in the Thevenin ECM, the expressions of the three matrices A_k^x , B_k^x , and C_k^x corresponding to estimating the battery SOC are as follows:

$$\begin{cases} A_k^x = \begin{pmatrix} 1 & 0 \\ 0 & e^{-T/\tau} \end{pmatrix} \\ B_k^x = \begin{pmatrix} -\frac{t}{C_0} \\ R_p (1 - e^{-T/\tau}) \end{pmatrix} \\ C_k^x = \begin{pmatrix} \frac{\partial u_{oc}}{\partial soc} & -1 \end{pmatrix} \Big|_{x_k = \hat{x}_k} \end{cases} \quad (24)$$

As the ohmic internal resistance serves as a descriptor of the SOH, it is crucial to construct the equations of state and observation to estimate the internal resistance. The state equation represents the updated value of the ohmic internal resistance considering external noise, while the observation equation aligns with the observation equation of the

first filter. The corresponding equations of state and observation for the ohmic resistance are provided below:

$$\begin{cases} R_o(k+1) = R_o(k) + r(k) \\ y_k = h(x_{k-1}, i_{k-1}) + v_k = U_{oc} - R_p i_k - u_k + v_k \end{cases} \quad (25)$$

With battery degradation, the ohmic internal resistance will gradually increase, and the noise $r(k)$ of the simulated internal resistance increase can be obtained from the changes of the internal resistance curve in the cyclic charge-discharge experiment. Therefore, A_k^R and C_k^R corresponding to the second filter can be described as follows:

$$\begin{cases} \hat{A}_k^R = 1 \\ \hat{C}_k^R = \left. \frac{\partial u_{oc}}{\partial R_o} \right|_{R_k=\hat{R}_k} = -i_k \end{cases} \quad (26)$$

Among them, A_k^R and C_k^R denote the matrices of state transfer and system measurement corresponding to the second extended Kalman filter, respectively. Therefore, the update process of Q and R in the EKF algorithm can be obtained as follows:

$$\begin{cases} \hat{Q}_{k+1} = (1 - d_k) \hat{Q}_k + d_k G \left(K_k \tilde{y}_{k+1} \tilde{y}_{k+1}^T K_k^T + P_{k+1|k} - A P_{k+1} A^T \right) G^T \\ G = (\Gamma^T \Gamma)^{-1} \\ \hat{R}_{k+1} = (1 - d_k) \hat{R}_k + d_k \tilde{y}_{k+1} \tilde{y}_{k+1}^T - C P_{k+1|k} A^T C^T \end{cases} \quad (27)$$

By summarizing the characteristics of the DAEKF algorithm, it can be seen that the calculated process of the FBC-DAEKF algorithm concludes with four steps [51]:

Step1: Initialize the parameters of FBC-DAEKF algorithm, as shown below.

$$\begin{cases} \hat{R}_o(0) = E[R_o(0)] \\ P_R(0) = E[(R_o(0) - \hat{R}_o(0))(R_o(0) - \hat{R}_o(0))^T] \\ \hat{x}(0) = E[x(0)] \\ P_x(0) = E[(x(0) - \hat{x}(0))(x(0) - \hat{x}(0))^T] \end{cases} \quad (28)$$

Step2: Predict the equations of state and covariance while estimating the SOC and the internal resistance. The calculation expressions are demonstrated below.

$$\begin{cases} R_o(k+1|k) = R_o(k|k) \\ P_R(k+1|k) = P_R(k|k) + \Gamma_R Q_R(k) \Gamma_R^T \\ x(k+1|k) = A_x(k)x(k|k) + B_x(k)i(k) \\ P_x(k+1|k) = A_x(k)\hat{P}_x(k|k)A_x^T(k) + \Gamma_x Q_x(k) \Gamma_x^T \end{cases} \quad (29)$$

Step3: Obtain the SOC Kalman gain and update the equations of state and covariance in SOC, as shown below.

$$\begin{cases} K_x(k+1) = P_x(k+1|k) C_x^T(k+1) [C_x(k+1) P_x(k+1|k) C_x^T(k+1) + R_x]^{-1} \\ \hat{x}(k+1|k+1) = x(k+1|k) + K_x(k+1) [y(k+1) - \hat{h}(k+1|k)] \\ P_x(k+1) = [I - K_x(k+1) C_x(k+1)] P_x(k+1|k) \\ SOC(k) = [1, 0]^T \hat{x}(k) \end{cases} \quad (30)$$

Step4: Update the Kalman gain and equations of state and covariance in R_o , as provided below.

$$\begin{cases} K_R(k+1) = P_R(k+1|k)C_R^T(k+1)[C_R(k+1)P_R(k+1|k)C_R^T(k+1) + R_R] \\ \hat{R}_o(k+1|k+1) = R_o(k+1|k) + K_R(k+1)\left[y(k+1) - \hat{h}(k+1|k)\right] \\ P_R(k+1) = [I - K_R(k+1)C_R(k+1)]P_R(k+1|k) \\ R_o(k) = \hat{R}_o(k) \end{cases} \quad (31)$$

Among them, Steps 2 to 4 are looped until the end of the algorithm. And in the cycle, Steps 3 and 4 are directly coupled with each other, so the estimated SOC and ohmic internal resistance at each moment can be continuously updated. The block diagram of the FBC-DAEKF algorithm is shown in Figure 2.

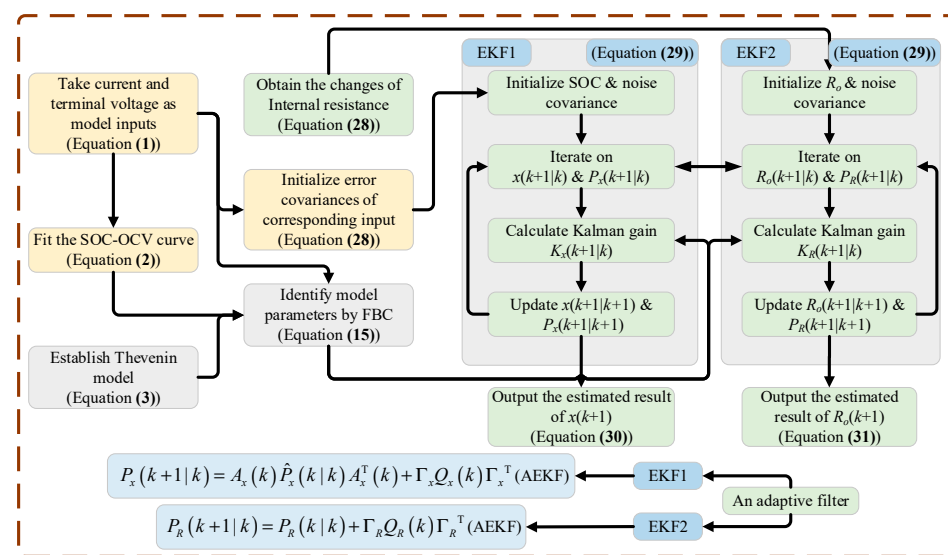


Figure 2. The block diagram of the FBC-DAEKF algorithm.

Within the estimation process, EKF1 refers to the filter utilized for the SOC estimation and the terminal voltage of the polarization resistance. On the other hand, EKF2 represents the filter employed for the ohmic internal resistance estimation. Throughout the estimation process, EKF1 and EKF2 interact with each other, exchanging information to rectify the estimation results. The voltage error generated by EKF1 serves as an input to EKF2.

3. Results

3.1. Experimental Platform and Corresponding Setup

In this research, a ternary lithium cell with a rated capacity of 70 Ah was employed for experiments, and all processes are performed under a charge-discharge tester and a thermostat. Furthermore, the experimental devices are connected to the host computer for data storage. The computer is configured with an Intel Core i7-8750 and an NVIDIA GeForce GTX 1060. The structure of the experimental platform is depicted in Figure 3.

The temperature for all experiments was maintained at 25 °C. In this study, the ground truth of SOC and Ro are obtained through the Hybrid Pulse Power Characterization (HPPC) test and the ampere hour integration method, respectively. Specifically, before conducting Beijing bus DST and DST experiments, the ground truth of Ro is obtained by analyzing the voltage curve of the HPPC test. In addition, before conducting the Beijing bus DST and DST experiments, the initial SOC of the battery is corrected through constant current charge-discharge tests, and the real-time calculated SOC based on the ampere hour integration method is used as the ground truth of SOC in the Beijing bus DST and DST experiments. Building upon the platform and corresponding setup, the corresponding experiments

can be performed. In this paper, the experiments conducted encompass Beijing bus DST and DST working conditions for the Li-ion batteries. These conditions were chosen to explore and analyze the diverse characteristics exhibited by Li-ion batteries under different operating scenarios. Among them, the terminal voltage and current curves under these conditions are demonstrated in Figure 4.

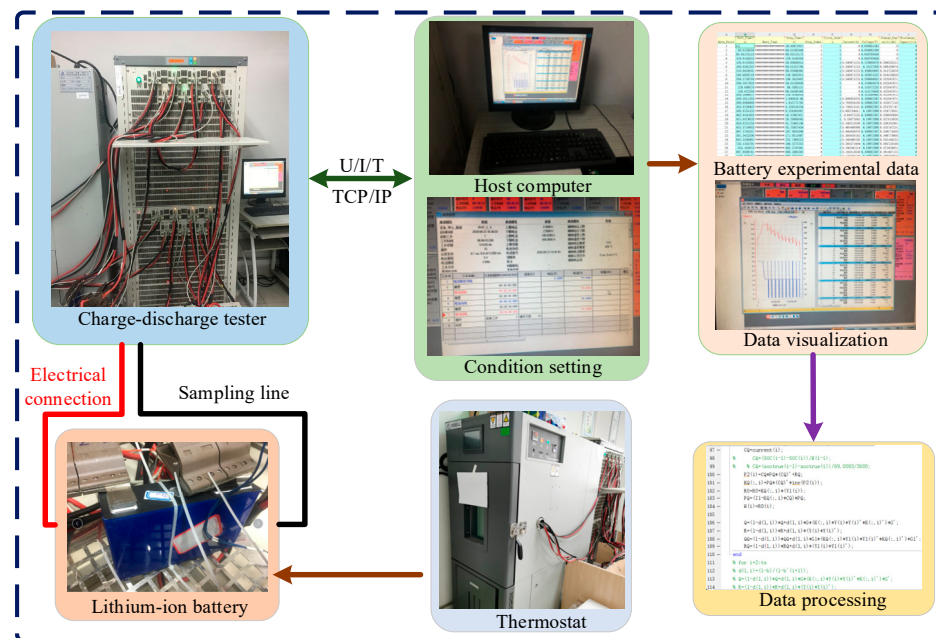


Figure 3. The structure of the experimental platform.

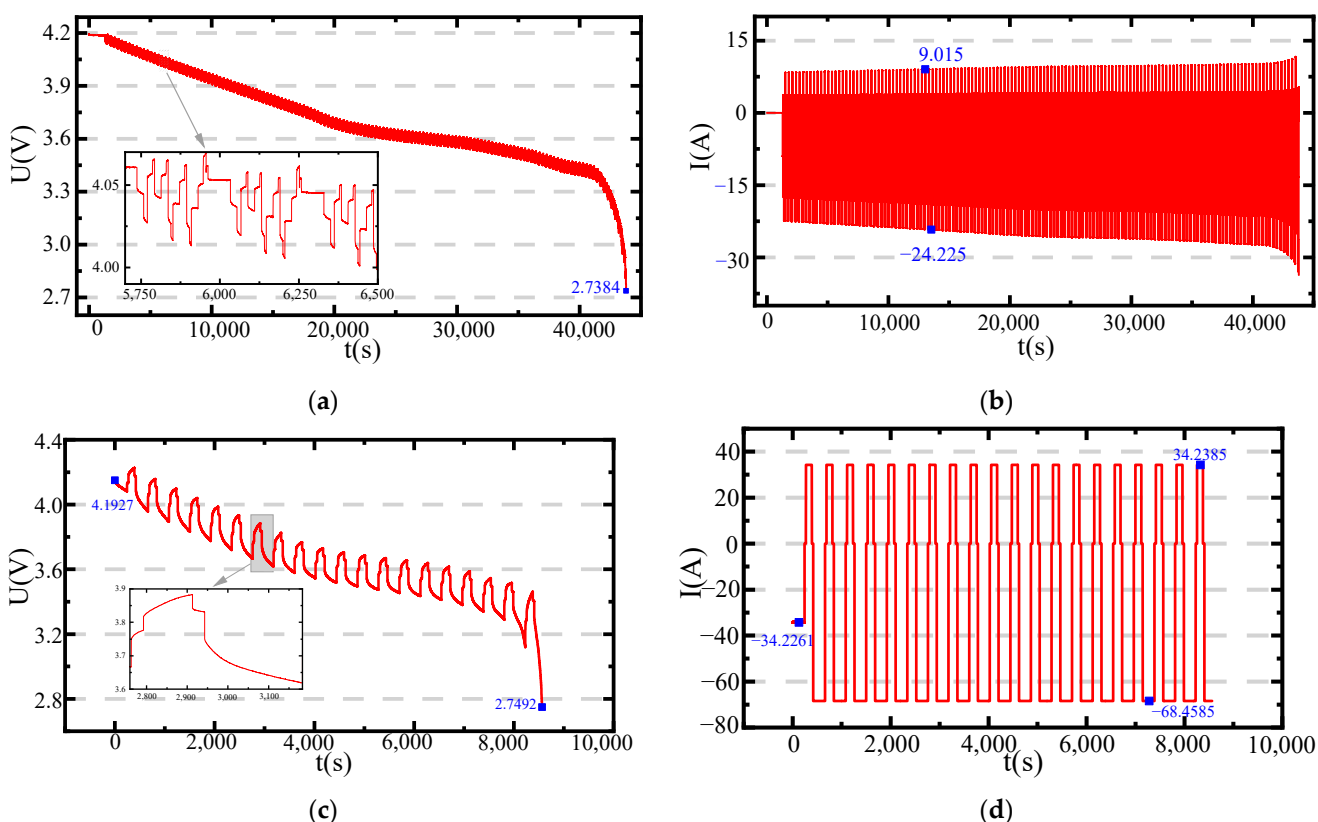


Figure 4. (a) Terminal voltage under the Beijing bus DST condition; (b) current under the Beijing bus DST condition; (c) terminal voltage under the DST condition; (d) current under the DST condition.

From Figure 4, it is evident that both the two working conditions are charge-discharge conditions, and the discharge rate and time are higher than those during charging. Therefore, it can be found that the battery voltage tends to decrease over time until it achieves the lower cut-off voltage.

3.2. Identification Results and Model Verification

The identification results of R_o , R_p , and C_p are obtained online using measured data and the FBC method. Under the Beijing bus DST condition, the identification results are shown in Figure 5.

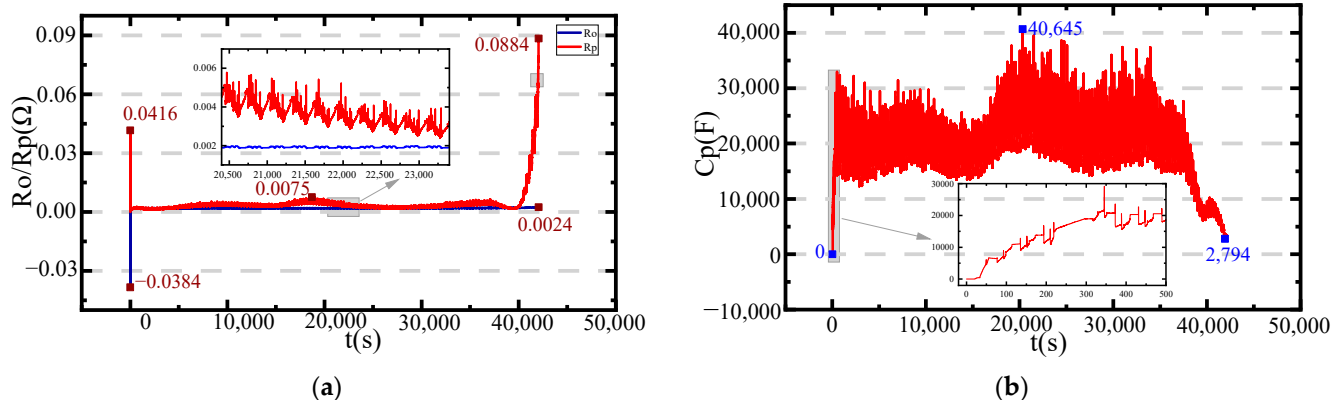


Figure 5. (a) Identification of R_o and R_p ; (b) identification of C_p .

Figure 5a represents the online identification results of R_o and R_p , from which it is evident that their identification values are very stable in the middle of the working condition. The sudden fluctuation in the early or late stage may be caused by the sudden change of the charge and discharge rate. Figure 5a represents the online identification result of C_p , from which it is evident that the identification results are relatively unstable, while the results are still within an acceptable range.

After obtaining the identification results, to verify the Thevenin ECM and prove the superiority of the developed parameter identification approach, the Beijing bus DST condition is employed as the working condition for simulating the terminal voltage. Under the Beijing bus DST condition, the simulated and measured terminal voltages and the corresponding errors between them are shown in Figure 6.

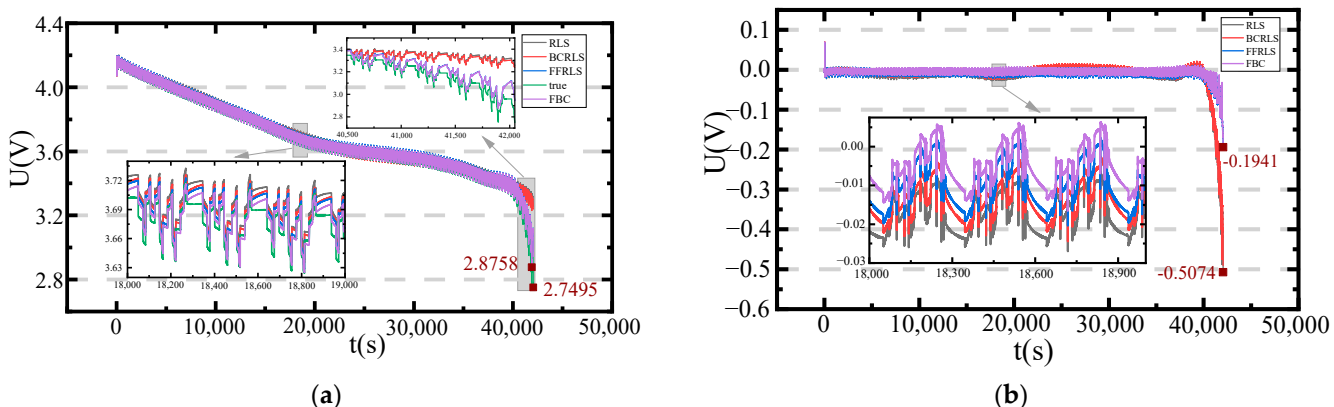


Figure 6. (a) Terminal voltages of diverse approaches; (b) Errors of diverse approaches.

Figure 6 illustrates that the simulated and measured curves almost coincide in the early and middle stages of the working condition. After data analysis, it can be seen that the MAEs of the RLS algorithm, bias compensation recursive least squares (BCRLS), FFFRLS algorithm, and FBC algorithm are 0.0153 V, 0.0131 V, 0.0088 V, and 0.0069 V, respectively,

which are lower than those of other identification approaches. By analyzing voltage MAEs, the aforementioned experimental results verify the superiority of the FBC method and the reliability of the Thevenin ECM, indicating that the proposed strategy can effectively reflect the battery characteristics under the Beijing bus DST condition.

3.3. Estimation Analysis under Complicated Conditions

To highlight the estimation superiority of the developed algorithm, three other algorithms are introduced to compare the results at 25 °C. Four algorithms are employed for the SOC estimation under Beijing bus DST and DST conditions. Assuming an initial SOC value of 0.95, the estimation results and corresponding errors are demonstrated in Figure 7.

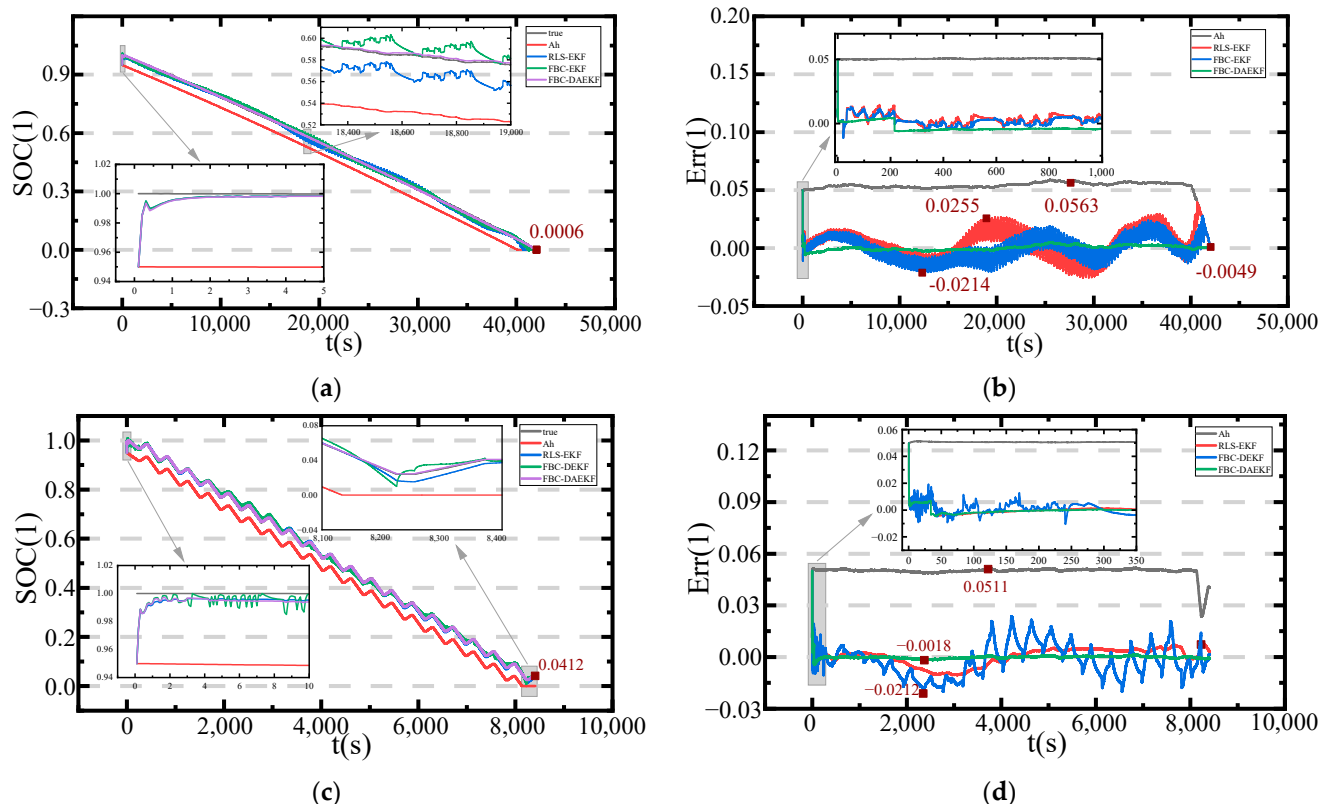


Figure 7. (a) Estimation results under the Beijing bus DST condition; (b) estimation errors under the Beijing bus DST condition; (c) estimation results under the DST condition; (d) estimation errors under the DST condition.

Figure 7a,c display the SOC estimation result curves under these two conditions. Meanwhile, Figure 7b,d depict the corresponding estimation error curves for both conditions. These four algorithms encompass the ampere-hour integration (Ah) method, the RLS-EKF method, the FBC-DEKF method, and the FBC-DAEKF method. The “true” label represents the true SOC value. In this study, the performance evaluation indicators include MAE and RMSE, which are described as follows:

$$\begin{cases} MAE = \frac{1}{n} \sum_{i=1}^n |Y_i - Y_{e,i}| \\ RMSE = \sqrt{\frac{1}{n} \sum_{i=1}^n (Y_i - Y_{e,i})^2} \end{cases} \quad (32)$$

Among them, n represents the number of sample points, Y_i represents the true value of SOC or R_o , and $Y_{e,i}$ represents the estimation value of SOC or R_o . Both of the above indicators are used to measure the estimation performance, but due to the square term used in RMSE, it is more sensitive to large errors. The performance evaluation indicators of the aforementioned four approaches for SOC estimation are described in Table 1.

Table 1. The SOC estimation evaluation indicators of the aforementioned approaches at 25 °C.

Algorithm Type	Beijing Bus DST Condition	DST Condition
Ah	RMSE: 5.38% MAE: 5.37% convergence time: ∞	RMSE: 4.97% MAE: 4.99% convergence time: ∞
RLS-EKF	RMSE: 1.89% MAE: 1.16% convergence time: 4 s	RMSE: 0.94% MAE: 0.76% convergence time: 8 s
FBC-DEKF	RMSE: 1.04% MAE: 0.82% convergence time: 4 s	RMSE: 0.88% MAE: 0.68% convergence time: 8 s
FBC-DAEKF	RMSE: 0.19% MAE: 0.17% convergence time: 4 s	RMSE: 0.07% MAE: 0.05% convergence time: 5 s

Table 1 demonstrates that the FBC-DAEKF algorithm outperforms the other algorithms in terms of error indicators such as convergence time, RMSE, and MAE for SOC estimation under both Beijing bus DST and DST conditions. With the SOC estimation results as a basis, the SOH under these two conditions can be estimated by utilizing the R_o to describe it [63,64]. The reference value of the internal resistance is represented by adopting the offline identification result with a value of 0.0019 Ω. Assuming an initial R_o value of 0.005 Ω, the convergence and estimation results of diverse approaches can be compared. At 25 °C, the estimation results and errors of these approaches are presented in Figure 8.

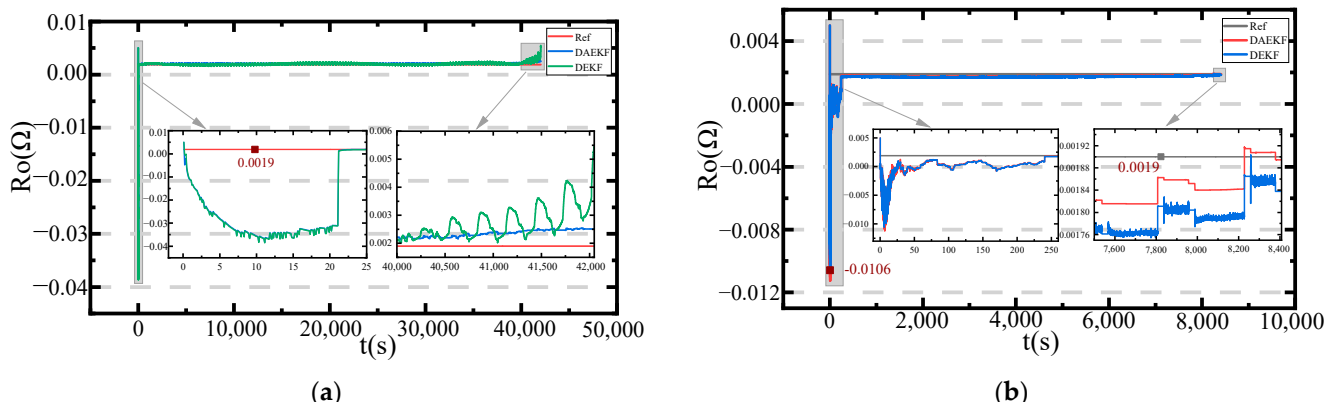
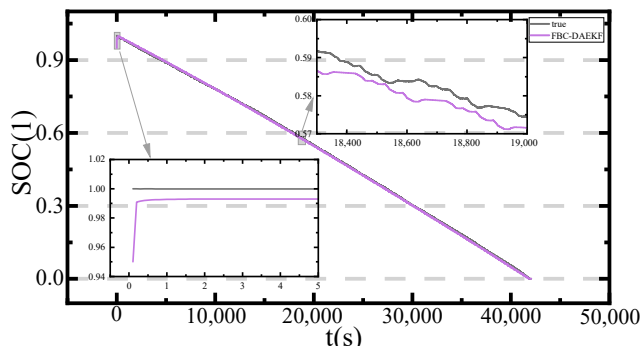
**Figure 8.** (a) Estimation results under the Beijing bus DST condition; (b) estimation results under the DST condition.

Figure 8a,b display the curves depicting the R_o estimation results under two conditions. Among them, before using the DEKF algorithm and the DAEKF algorithm to estimate R_o , the FBC algorithm is required for parameter identification. Moreover, the “Ref” label denotes the reference R_o value. In Figure 8a, the increase in R_o is caused by the lower SOC. The performance evaluation indicators of the aforementioned approaches for R_o estimation are summarized in Table 2.

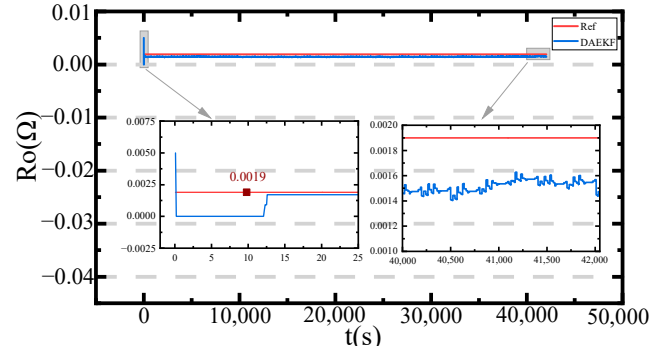
Table 2 confirms that the developed algorithm outperforms the FBC-DEKF algorithm in terms of error indicators such as RMSE and MAE for the estimation of the R_o under both Beijing bus DST and DST conditions, as well. These results serve as evidence for the accuracy and superiority of the developed algorithm in estimating the SOC and ohmic internal resistance. To verify the effectiveness of the proposed algorithm at different temperatures, the estimation results under the Beijing bus DST working conditions at 35 °C and 15 °C are shown in Figure 9.

Table 2. The R_o estimation evaluation indicators of the aforementioned approaches at 25 °C.

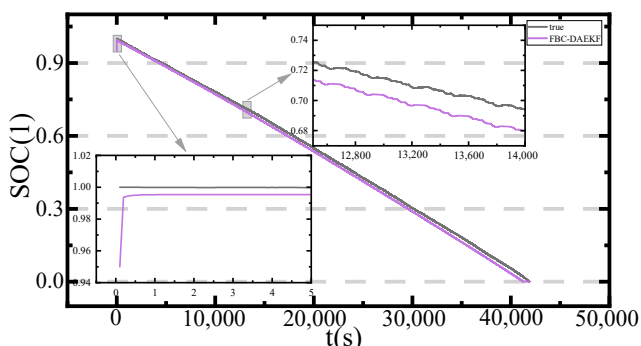
Algorithm Type	Beijing Bus DST Condition	DST Condition
FBC-DEKF	RMSE: 0.078% MAE: 0.017% convergence time: 23 s	RMSE: 0.043% MAE: 0.022% convergence time: 240 s
FBC-DAEKF	RMSE: 0.075% MAE: 0.018% convergence time: 23 s	RMSE: 0.043% MAE: 0.014% convergence time: 240 s



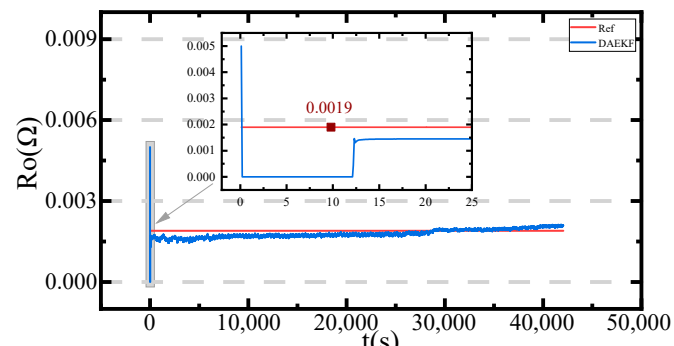
(a)



(b)



(c)



(d)

Figure 9. (a) SOC estimation results at 35 °C; (b) R_o estimation results at 35 °C; (c) SOC estimation results at 15 °C; (d) R_o estimation results at 15 °C.

From Figure 9, it is evident that the estimation results of SOC and R_o are in an acceptable range at 35 °C and 15 °C as well. The performance evaluation indicators of the proposed method for estimation are demonstrated in Table 3.

Table 3 demonstrates that at 35 °C and 15 °C, the developed method also performs well in terms of two error indicators for the estimation of SOC and R_o , which verifies the FBC-DAEKF algorithm at diverse temperatures. In addition, under the DST condition and the Beijing bus DST condition, the overall estimated time at each sampling point is approximately 0.0001 s. Among them, the FBC algorithm takes approximately 0.00007 s, and the DAEKF algorithm takes approximately 0.00003 s. In this article, the sampling point interval time is 0.1 s.

Table 3. The estimation evaluation indicators of the proposed method at 35 °C and 15 °C.

Temperature	Estimation Type	Beijing Bus DST Condition
15 °C	SOC	RMSE: 1.31% MAE: 1.32% convergence time: 1 s
	R_o	RMSE: 0.011% MAE: 0.016% convergence time: 13 s
25 °C	SOC	RMSE: 0.19% MAE: 0.17% convergence time: 4 s
	R_o	RMSE: 0.075% MAE: 0.018% convergence time: 23 s
35 °C	SOC	RMSE: 0.182% MAE: 0.324% convergence time: 1 s
	R_o	RMSE: 0.044% MAE: 0.045% convergence time: 13 s

4. Conclusions

In this study, an online parameter identification method named FBC and a DAEKF algorithm are developed to form an efficient co-estimation algorithm called the FBC-DAEKF algorithm by combining them. The novel co-estimation method is employed to estimate the SOC and SOH of EV batteries, considering the problems of data saturation, the interference of colored noise, and the changes in observation noise. Under the Beijing bus DST condition of 25 °C, the MAE, the RMSE, and the convergence time of SOC estimation are 0.17%, 0.19%, and 4 s, respectively, with the corresponding values of 0.018%, 0.075%, and 23 s for internal resistance estimation. In addition, under the DST condition of 25 °C, the MAE, the RMSE and the convergence time of SOC estimation are 0.05%, 0.07% and 5 s, respectively, with the corresponding data of 0.014%, 0.043%, and 240 s for internal resistance estimation. Accurate SOC and SOH estimation is crucial for ensuring the safe and efficient operation of EVs. The FBC-DAKEF algorithm has proven to be effective in mitigating the issues that arise from incorrect SOC and SOH estimation. By employing this algorithm, potential problems associated with inaccurate SOC and SOH can be effectively avoided, thereby enhancing the overall performance and reliability of EVs.

Author Contributions: Conceptualization, R.X., S.W. and F.F.; Methodology, R.X.; Software, R.X.; Validation, R.X.; Formal analysis, S.W.; Investigation, R.X., S.W., C.Y., Y.F., W.C. and C.F.; Resources, R.X., C.Y., Y.F. and C.F.; Data curation, R.X., F.F., C.Y. and Y.F.; Writing—original draft, R.X.; Writing—review and editing, R.X., S.W. and F.F.; Visualization, F.F. and W.C.; Supervision, S.W., F.F. and C.Y.; Project administration, S.W. and F.F.; Funding acquisition, S.W. All authors have read and agreed to the published version of the manuscript.

Funding: This research was funded by the National Natural Science Foundation of China (No. 61801407) and the Chongqing Natural Science Foundation (No. CSTB2023NSCQ-MSX0359).

Data Availability Statement: Not applicable.

Conflicts of Interest: The authors declare no conflict of interest.

References

- Chen, Y.; Huang, D.; Zhu, Q.; Liu, W.; Liu, C.; Xiong, N. A new state of charge estimation algorithm for lithium-ion batteries based on the fractional unscented Kalman filter. *Energies* **2017**, *10*, 1313. [[CrossRef](#)]
- Sun, F. Green Energy and Intelligent Transportation—promoting green and intelligent mobility. *Green Energy Intell. Transp.* **2022**, *1*, 100017. [[CrossRef](#)]

3. Li, X.; Huang, Z.; Tian, J.; Tian, Y. State-of-charge estimation tolerant of battery aging based on a physics-based model and an adaptive cubature Kalman filter. *Energy* **2021**, *220*, 119767. [[CrossRef](#)]
4. Mawonou, K.S.R.; Eddahech, A.; Dumur, D.; Beauvois, D.; Godoy, E. Improved state of charge estimation for Li-ion batteries using fractional order extended Kalman filter. *J. Power Sources* **2019**, *435*, 226710. [[CrossRef](#)]
5. Jia, Y.; Luo, G.; Zhang, Y. Development of optimal speed trajectory control strategy for electric vehicles to suppress battery aging. *Green Energy Intell. Transp.* **2022**, *1*, 100030. [[CrossRef](#)]
6. Xiong, R.; Kim, J.; Shen, W.; Lv, C.; Li, H.; Zhu, X.; Zhao, W.; Gao, B.; Guo, H.; Zhang, C.; et al. Key technologies for electric vehicles. *Green Energy Intell. Transp.* **2022**, *1*, 100041. [[CrossRef](#)]
7. Farzin, H.; Fotuhi-Firuzabad, M.; Moeini-Aghaie, M. A practical scheme to involve degradation cost of lithium-ion batteries in vehicle-to-grid applications. *IEEE Trans. Sustain. Energy* **2016**, *7*, 1730–1738. [[CrossRef](#)]
8. Feng, F.; Yang, R.; Meng, J.; Xie, Y.; Zhang, Z.; Chai, Y.; Mou, L. Electrochemical impedance characteristics at various conditions for commercial solid–liquid electrolyte lithium-ion batteries: Part 1. experiment investigation and regression analysis. *Energy* **2022**, *242*, 122880. [[CrossRef](#)]
9. Ling, L.; Wei, Y. State-of-charge and state-of-health estimation for lithium-ion batteries based on dual fractional-order extended Kalman filter and online parameter identification. *IEEE Access* **2021**, *9*, 47588–47602. [[CrossRef](#)]
10. Zhang, Y.; Feng, F.; Wang, S.; Meng, J.; Xie, J.; Ling, R.; Yin, H.; Zhang, K.; Chai, Y. Joint nonlinear-drift-driven Wiener process-Markov chain degradation switching model for adaptive online predicting lithium-ion battery remaining useful life. *Appl. Energy* **2023**, *341*, 121043. [[CrossRef](#)]
11. Zhu, X.; Macía, L.F.; Jaguemont, J.; de Hoog, J.; Nikolian, A.; Omar, N.; Hubin, A. Electrochemical impedance study of commercial LiNi0.80Co0.15Al0.05O2 electrodes as a function of state of charge and aging. *Electrochim. Acta* **2018**, *287*, 10–20. [[CrossRef](#)]
12. Jin, G.; Li, L.; Xu, Y.; Hu, M.; Fu, C.; Qin, D. Comparison of SOC estimation between the integer-order model and fractional-order model under different operating conditions. *Energies* **2020**, *13*, 1785. [[CrossRef](#)]
13. Chen, Z.; Yang, L.; Zhao, X.; Wang, Y.; He, Z. Online state of charge estimation of Li-ion battery based on an improved unscented Kalman filter approach. *Appl. Math. Model.* **2019**, *70*, 532–544. [[CrossRef](#)]
14. Muhammad, N.P.A.; Artono, D.S.; Hendri, W. Design a battery management system (BMS) with an automatic cut off system on LFP (LiFePO₄) battery type for powerbank application. *J. Phys. Conf. Ser.* **2021**, *1825*, 012038.
15. Ran, X.; Shunli, W.; Carlos, F.; Chunmei, Y.; Yongcun, F.; Wen, C.; Cong, J. A novel joint estimation method of state of charge and state of health based on the strong tracking-dual adaptive extended Kalman filter algorithm for the electric vehicle lithium-ion batteries. *Int. J. Electrochem. Sci.* **2021**, *16*, 211114.
16. Cai, M.; Chen, W.; Tan, X. Battery state-of-charge estimation based on a dual unscented Kalman filter and fractional variable-order model. *Energies* **2017**, *10*, 1577. [[CrossRef](#)]
17. Li, J.; Lai, Q.; Wang, L.; Lyu, C.; Wang, H. A method for SOC estimation based on simplified mechanistic model for LiFePO₄ battery. *Energy* **2016**, *114*, 1266–1276. [[CrossRef](#)]
18. Luo, Y.; Qi, P.; Kan, Y.; Huang, J.; Huang, H.; Luo, J.; Wang, J.; Wei, Y.; Xiao, R.; Zhao, S. State of charge estimation method based on the extended Kalman filter algorithm with consideration of time-varying battery parameters. *Int. J. Energy Res.* **2020**, *44*, 10538–10550. [[CrossRef](#)]
19. Liu, K.; Hu, X.; Yang, Z.; Xie, Y.; Feng, S. Lithium-ion battery charging management considering economic costs of electrical energy loss and battery degradation. *Energy Convers. Manag.* **2019**, *195*, 167–179. [[CrossRef](#)]
20. Xiaosong, H.; Kai, Z.; Kailong, L. Advanced fault diagnosis for lithium-ion battery systems: A review of fault mechanisms, fault features, and diagnosis procedures. *IEEE Ind. Electron. Mag.* **2020**, *14*, 65–91.
21. Fan, Y.; Bao, Y.; Ling, C.; Chu, Y.; Tan, X.; Yang, S. Experimental study on the thermal management performance of air cooling for high energy density cylindrical lithium-ion batteries. *Appl. Therm. Eng.* **2019**, *155*, 96–109. [[CrossRef](#)]
22. Feng, F.; Hu, X.; Hu, L.; Hu, F.; Li, Y.; Zhang, L. Propagation mechanisms and diagnosis of parameter inconsistency within Li-Ion battery packs. *Renew. Sustain. Energy Rev.* **2019**, *112*, 102–113. [[CrossRef](#)]
23. Xu, J.; Sun, C.; Ni, Y.; Lyu, C.; Wu, C.; Zhang, H.; Yang, Q.; Feng, F. Fast identification of micro-health parameters for retired batteries based on a simplified P2D model by using padé approximation. *Batteries* **2023**, *9*, 64. [[CrossRef](#)]
24. Ren, H.; Zhao, Y.; Chen, S.; Wang, T. Design and implementation of a battery management system with active charge balance based on the SOC and SOH online estimation. *Energy* **2019**, *166*, 908–917. [[CrossRef](#)]
25. Feng, F.; Song, B.; Xu, J.; Na, W.; Zhang, K.; Chai, Y. Multiple time scale state-of-charge and capacity-based equalisation strategy for lithium-ion battery pack with passive equaliser. *J. Energy Storage* **2022**, *53*, 105196. [[CrossRef](#)]
26. Park, J.; Lee, M.; Kim, G.; Park, S.; Kim, J. Integrated approach based on dual extended Kalman filter and multivariate autoregressive model for predicting battery capacity using health indicator and SOC/SOH. *Energies* **2020**, *13*, 2138. [[CrossRef](#)]
27. Chang, C.; Zheng, Y.; Yu, Y. Estimation for battery state of charge based on temperature effect and fractional extended Kalman filter. *Energies* **2020**, *13*, 5947. [[CrossRef](#)]
28. Lashway, C.R.; Mohammed, O.A. Adaptive battery management and parameter estimation through physics-based modeling and experimental verification. *IEEE Trans. Transp. Electrif.* **2016**, *2*, 454–464. [[CrossRef](#)]
29. Ahmad, A.B.; Ooi, C.A.; Ishak, D.; Teh, J. State-of-charge balancing control for on/off-line internal cells using hybrid modular multi-level converter and parallel modular dual L-bridge in a grid-scale battery energy storage system. *IEEE Access* **2019**, *7*, 131–147. [[CrossRef](#)]

30. Zhang, J.; Wang, P.; Liu, Y.; Cheng, Z. Variable-order equivalent circuit modeling and state of charge estimation of lithium-ion battery based on electrochemical impedance spectroscopy. *Energies* **2021**, *14*, 769. [[CrossRef](#)]
31. Stroe, D.-I.; Swierczynski, M.; Stroe, A.-I.; Kaer, S.K.; Teodorescu, R. Lithium-ion battery power degradation modelling by electrochemical impedance spectroscopy. *IET Renew. Power Gener.* **2017**, *11*, 1136–1141. [[CrossRef](#)]
32. Westerhoff, U.; Kroker, T.; Kurbach, K.; Kurrat, M. Electrochemical impedance spectroscopy based estimation of the state of charge of lithium-ion batteries. *J. Energy Storage* **2016**, *8*, 244–256. [[CrossRef](#)]
33. Feng, F.; Yang, R.; Meng, J.; Xie, Y.; Zhang, Z.; Chai, Y.; Mou, L. Electrochemical impedance characteristics at various conditions for commercial solid–liquid electrolyte lithium-ion batteries: Part. 2. Modeling and prediction. *Energy* **2022**, *243*, 123091. [[CrossRef](#)]
34. Chen, C.; Xiong, R.; Yang, R.; Li, H. A novel data-driven method for mining battery open-circuit voltage characterization. *Green Energy Intell. Transp.* **2022**, *1*, 100001. [[CrossRef](#)]
35. Sheng, H.; Xiao, J. Electric vehicle state of charge estimation: Nonlinear correlation and fuzzy support vector machine. *J. Power Sources* **2015**, *281*, 131–137. [[CrossRef](#)]
36. Sun, X.; Zhong, K.; Han, M. A hybrid prognostic strategy with unscented particle filter and optimized multiple kernel relevance vector machine for lithium-ion battery. *Measurement* **2021**, *170*, 108679. [[CrossRef](#)]
37. Xiaojun, T.; Di, Z.; Pengxiang, L.; Jun, R.; Yuqian, F. Online state-of-health estimation of lithium-ion battery based on dynamic parameter identification at multi timescale and support vector regression. *J. Power Sources* **2021**, *484*, 229233. [[CrossRef](#)]
38. Bin, X.; Bing, X.; Luoshi, L. Rapid measurement method for lithium-ion battery state of health estimation based on least squares support vector regression. *Int. J. Energy Res.* **2020**, *45*, 5695–5709.
39. Ruhatiya, C.; Gandra, R.; Kondaiah, P.; Manivas, K.; Samhith, A.; Gao, L.; Lam, J.S.L.; Garg, A. Intelligent optimization of bioleaching process for waste lithium-ion batteries: An application of support vector regression approach. *Int. J. Energy Res.* **2020**, *45*, 6152–6162. [[CrossRef](#)]
40. Jia, J.; Liang, J.; Shi, Y.; Wen, J.; Pang, X.; Zeng, J. SOH and RUL prediction of lithium-ion batteries based on Gaussian process regression with indirect health indicators. *Energies* **2020**, *13*, 375. [[CrossRef](#)]
41. Tian, Y.; Lai, R.; Li, X.; Xiang, L.; Tian, J. A combined method for state-of-charge estimation for lithium-ion batteries using a long short-term memory network and an adaptive cubature Kalman filter. *Appl. Energy* **2020**, *265*, 114789. [[CrossRef](#)]
42. Xia, B.; Cui, D.; Sun, Z.; Lao, Z.; Zhang, R.; Wang, W.; Sun, W.; Lai, Y.; Wang, M. State of charge estimation of lithium-ion batteries using optimized Levenberg–Marquardt wavelet neural network. *Energy* **2018**, *153*, 694–705. [[CrossRef](#)]
43. Jiménez-Bermejo, D.; Fraile-Ardanuy, J.; Castaño-Solis, S.; Merino, J.; Alvaro-Hermana, R. Using dynamic neural networks for battery state of charge estimation in electric vehicles. *Procedia Comput. Sci.* **2018**, *130*, 533–540. [[CrossRef](#)]
44. Jiao, M.; Wang, D.; Qiu, J. A GRU-RNN based momentum optimized algorithm for SOC estimation. *J. Power Sources* **2020**, *459*, 228051. [[CrossRef](#)]
45. Hicham, C.; Christopher, I.E.C. State of charge and state of health estimation for lithium batteries using recurrent neural networks. *IEEE Trans. Veh. Technol.* **2017**, *66*, 8773–8783.
46. Chemali, E.; Kollmeyer, P.J.; Preindl, M.; Emadi, A. State-of-charge estimation of Li-ion batteries using deep neural networks: A machine learning approach. *J. Power Sources* **2018**, *400*, 242–255. [[CrossRef](#)]
47. Li, C.; Xiao, F.; Fan, Y. An approach to state of charge estimation of lithium-ion batteries based on recurrent neural networks with gated recurrent unit. *Energies* **2019**, *12*, 1592. [[CrossRef](#)]
48. Zhou, Z.; Liu, Y.; You, M.; Xiong, R.; Zhou, X. Two-stage aging trajectory prediction of LFP lithium-ion battery based on transfer learning with the cycle life prediction. *Green Energy Intell. Transp.* **2022**, *1*, 100008. [[CrossRef](#)]
49. Dai, H.; Zhao, G.; Lin, M.; Wu, J.; Zheng, G. A novel estimation method for the state of health of lithium-ion battery using prior knowledge-based neural network and Markov chain. *IEEE Trans. Ind. Electron.* **2019**, *66*, 7706–7716. [[CrossRef](#)]
50. Zhang, R.; Li, X.; Sun, C.; Yang, S.; Tian, Y.; Tian, J. State of charge and temperature joint estimation based on ultrasonic reflection waves for lithium-ion battery applications. *Batteries* **2023**, *9*, 335. [[CrossRef](#)]
51. Li, J.; Ye, M.; Gao, K.; Xu, X.; Wei, M.; Jiao, S. Joint estimation of state of charge and state of health for lithium-ion battery based on dual adaptive extended Kalman filter. *Int. J. Energy Res.* **2021**, *45*, 13307–13322. [[CrossRef](#)]
52. Zhu, Q.; Xu, M.; Liu, W.; Zheng, M. A state of charge estimation method for lithium-ion batteries based on fractional order adaptive extended kalman filter. *Energy* **2019**, *187*, 115880. [[CrossRef](#)]
53. Li, Y.; Chen, J.; Lan, F. Enhanced online model identification and state of charge estimation for lithium-ion battery under noise corrupted measurements by bias compensation recursive least squares. *J. Power Sources* **2020**, *456*, 227984. [[CrossRef](#)]
54. Ouyang, T.; Xu, P.; Chen, J.; Lu, J.; Chen, N. Improved parameters identification and state of charge estimation for lithium-ion battery with real-time optimal forgetting factor. *Electrochim. Acta* **2020**, *353*, 136576. [[CrossRef](#)]
55. Lin, Q.; Li, X.; Tu, B.; Cao, J.; Zhang, M.; Xiang, J. Stable and accurate estimation of SOC using eXogenous Kalman filter for lithium-ion batteries. *Sensors* **2023**, *23*, 467. [[CrossRef](#)] [[PubMed](#)]
56. Yi, S.; Zorzi, M. Robust Kalman filtering under model uncertainty: The case of degenerate densities. *IEEE Trans. Autom. Control* **2022**, *67*, 3458–3471. [[CrossRef](#)]
57. Sahri, Y.; Belkhier, Y.; Tamalouzt, S.; Ullah, N.; Shaw, R.N.; Chowdhury, M.S.; Techato, K. Energy management system for hybrid PV/wind/battery/fuel cell in microgrid-based hydrogen and economical hybrid battery/super capacitor energy storage. *Energies* **2021**, *14*, 5722. [[CrossRef](#)]
58. Yi, S.; Zorzi, M. Robust fixed-lag smoothing under model perturbations. *J. Frankl. Inst.* **2023**, *360*, 458–483. [[CrossRef](#)]

59. Tang, A.; Jiang, Y.; Yu, Q.; Zhang, Z. A hybrid neural network model with attention mechanism for state of health estimation of lithium-ion batteries. *J. Energy Storage* **2023**, *68*, 107734. [[CrossRef](#)]
60. Yang, Y.; Zhao, L.; Yu, Q.; Liu, S.; Zhou, G.; Shen, W. State of charge estimation for lithium-ion batteries based on cross-domain transfer learning with a feedback mechanism. *J. Energy Storage* **2023**, *70*, 108037. [[CrossRef](#)]
61. Yu, Q.; Liu, Y.; Long, S.; Jin, X.; Li, J.; Shen, W. A branch current estimation and correction method for a parallel connected battery system based on dual BP neural networks. *Green Energy Intell. Transp.* **2022**, *1*, 100029. [[CrossRef](#)]
62. Jialu, Q.; Shunli, W.; Chunmei, Y.; Weihao, S.; Carlos, F. A novel bias compensation recursive least square-multiple weighted dual extended Kalman filtering method for accurate state-of-charge and state-of-health co-estimation of lithium-ion batteries. *Int. J. Circuit Theory Appl.* **2021**, *49*, 3879–3893.
63. Gholizadeh, M.; Yazdizadeh, A. Systematic mixed adaptive observer and EKF approach to estimate SOC and SOH of lithium-ion battery. *IET Electr. Syst. Transp.* **2020**, *10*, 135–143. [[CrossRef](#)]
64. Wassiliadis, N.; Adermann, J.; Frericks, A.; Pak, M.; Reiter, C.; Lohmann, B.; Lienkamp, M. Revisiting the dual extended Kalman filter for battery state-of-charge and state-of-health estimation: A use-case life cycle analysis. *J. Energy Storage* **2018**, *19*, 73–87. [[CrossRef](#)]

Disclaimer/Publisher's Note: The statements, opinions and data contained in all publications are solely those of the individual author(s) and contributor(s) and not of MDPI and/or the editor(s). MDPI and/or the editor(s) disclaim responsibility for any injury to people or property resulting from any ideas, methods, instructions or products referred to in the content.